Applied Surface Science 712 (2025) 164200

Contents lists available at ScienceDirect

Applied Surface Science

journal homepage: www.elsevier.com/locate/apsusc

Full Length Article

Polymer derived tribofilm on silicon-doped diamond-like carbon coatings

Takeru Omiya [a,b,c,*], Alexander Welle [d], Manuel Evaristo [a], Pooja Sharma [a], Albano Cavaleiro [a,c], Arménio C. Serra [b], Jorge F.J. Coelho [b,c], Maria Clelia Righi [e,**], Fabio Ferreira [a,c,*]

[a] University of Coimbra, CEMMPRE, ARISE, Department of Mechanical Engineering, Rua Luís Reis Santos, 3030-788 Coimbra, Portugal
[b] University of Coimbra, CEMMPRE, ARISE, Department of Chemical Engineering, Rua Silvio Lima, 3030-790 Coimbra, Portugal
[c] Laboratory for Wear, Testing & Materials, Instituto Pedro Nunes, Rua Pedro Nunes, 3030-199 Coimbra, Portugal
[d] Karlsruhe Nano Micro Facility, and Institute of Functional Interfaces (IFG), Karlsruhe Institute of Technology (KIT), 76344 Eggenstein-Leopoldshafen, Germany
[e] Department of Physics and Astronomy, University of Bologna, Bologna 40127, Italy

ARTICLE INFO

Keywords:
Nanotribology
Silicon-doped diamond-like carbon
Block copolymer
Nanoscale tribofilm
N–Si chemisorption
Boundary lubrication

ABSTRACT

Metal-free polymer additives used in conjunction with diamond-like carbon (DLC) coatings offer an environmentally sustainable approach for reducing friction and wear under boundary lubrication. In this study, a functionalized block copolymer, poly(lauryl methacrylate)-block-poly(2-dimethylaminoethyl methacrylate) (PLMA-*b*-PDMAEMA), is investigated as a friction modifier for silicon-doped DLC (Si-DLC) coatings. Tribological tests reveal that this copolymer significantly lowers friction compared to both a PLMA homopolymer and the base oil alone. ToF-SIMS, synchrotron-based XPS, and cross-sectional FIB-TEM analyses confirm the in-situ formation of a robust tribofilm, with a thickness of approximately 5–12 nm. Depth-resolved chemical analysis reveals a stratified structure in which the PDMAEMA segment chemisorbs onto reactive silicon sites via N–Si bonds, while the PLMA alkyl chains form a low-shear, oleophilic outer interface. The tribofilm remains intact after sliding under a Hertzian contact pressure of approximately 1 gigapascal, indicating excellent mechanical resilience. These findings demonstrate that molecular-level design of copolymers enables strong substrate anchoring and friction reduction without the use of metals, phosphorus, or sulfur. The mechanistic insights gained from this work provide design principles for next-generation, sustainable lubricant additives capable of forming self-assembled, nanoscale tribofilms on reactive DLC surfaces under demanding conditions.

1. Introduction

Controlling friction and wear in mechanical systems is critical to improving energy efficiency, reducing emissions, and extending component lifetimes [1–3]. Traditionally, lubricant additives such as zinc dialkyldithiophosphates (ZnDTPs) and molybdenum dithiocarbamates (MoDTCs) have been widely used to protect surfaces under boundary lubrication conditions by forming tribofilms that prevent direct metal-to-metal contact [4–7]. However, the environmental impacts and catalyst poisoning associated with phosphorus- and sulfur-containing additives have prompted the development of more sustainable, metal-free alternatives [8,9].

Polymeric additives offer a promising route to overcome these challenges. In particular, copolymers can be tailored at the molecular level to improve viscosity, increase adsorption, and achieve better tribological performance [10,11]. By incorporating functional groups into specific segments of the polymer chain, stable and protective adsorbed layers can be formed on substrates, that can reduce friction without relying on phosphorus or sulfur compounds [12,13]. In particular, poly(methacrylate) based copolymers with functional groups such as amines or hydroxyls have been designed to form boundary films through physical adsorption and chemical interactions with the steel surface [14–16]. These copolymers have demonstrated improved friction and wear performance under mixed and boundary lubrication regimes by anchoring to oxide layers on steel. Functionalized copolymers have been successfully applied to steel surfaces, and more recently, they have been explored for use with diamond-like carbon (DLC) films, which are characterized by high hardness, low friction, and excellent wear

* Corresponding authors at: University of Coimbra, CEMMPRE, ARISE, Department of Mechanical Engineering, Rua Luís Reis Santos, 3030-788 Coimbra, Portugal.
** Corresponding author at: Department of Physics and Astronomy, University of Bologna, Bologna 40127, Italy.
E-mail addresses: takeru.omiya@student.dem.uc.pt (T. Omiya), clelia.righi@unibo.it (M.C. Righi), fabio.ferreira@dem.uc.pt (F. Ferreira).

https://doi.org/10.1016/j.apsusc.2025.164200
Received 31 May 2025; Received in revised form 26 July 2025; Accepted 28 July 2025
Available online 5 August 2025

resistance [17]. Among various types of DLC, silicon-doped DLC (Si-DLC) has attracted increasing attention due to its enhanced surface reactivity and improved compatibility with lubricant additives [18]. Recent studies suggest that Si-DLC surfaces are more amenable to adsorption and tribofilm formation by polar or functionalized polymeric additives, leading to better friction-reducing and anti-wear performance [19,20]. In the study, the poly(lauryl methacrylate)-block-poly(2-(dimethylamino)ethyl methacrylate) (PLMA-*b*-PDMAEMA) was investigated, which was specifically designed to combine excellent solubility in base oils (through the nonpolar PLMA block) with a high density of amine functional groups (in the PDMAEMA block) capable of interacting strongly with Si-DLC surfaces. This molecular architecture enables selective adsorption and tribofilm formation via N–Si bonding, offering a new strategy for phosphorus-free lubrication on functionalized DLC surfaces.

However, the detailed chemical composition and bonding states of these tribofilms remain unclear. A better understanding of these aspects is essential to elucidate the mechanisms by which functionalized copolymers reduce friction and wear. In this work, tribological tests and advanced surface analysis techniques, including time-of-flight secondary ion mass spectrometry (ToF-SIMS) and synchrotron-based X-ray photoelectron spectroscopy (XPS), are employed to identify key chemical markers, determine the binding states within the tribofilm, and establish correlations between the molecular structure of the PLMA-*b*-PDMAEMA, tribofilm formation, and the resulting friction and wear characteristics. The knowledge gained from this work will support the rational design of next-generation, environmentally friendly lubrication systems that utilize functionalized copolymers for improved performance on doped DLC coatings.

2. Materials and methods

2.1. Coatings

The DLC coatings were deposited on M2 steel disks (50 mm diameter, 801 Vickers hardness), referring to previous studies [18]. The steel samples, polished to a surface roughness (Ra) of ~100 nm, underwent deposition in a Teer Coatings unbalanced magnetron sputtering system. This system employed four targets: pure chromium, pure graphite (two targets), and pure silicon. A 300 nm chromium interlayer was deposited first to enhance adhesion. For Si-DLC coatings, the power on graphite targets remained constant, while the silicon content was varied by adjusting the power on the silicon target. All DLC coatings were approximately 1 μm thick, based on cross-sectional scanning electron microscope (SEM) analysis conducted on Si substrates. The coating composition was evaluated using SEM with energy-dispersive X-ray spectroscopy. The film hardness and Young's modulus were measured using a Micromaterials Nanotest platform equipped with a Berkovich indenter, applying a maximum load of 10 mN. The measurements were performed at 16 different locations on each sample, and the average values and standard deviations were calculated to ensure statistical reliability. Surface morphology was analyzed by AFM (Innova Veeco) in tapping mode with specific scan settings. Properties of the coatings are summarized in Table 1, demonstrating trends in roughness, hardness, Young's modulus, and sp^3 content with varying Si content. The sp^3 content of the DLC film was evaluated based on the full width at half maximum (FWHM) of the G peak obtained from Raman spectroscopy [21,22].

Table 1
Physical and structural properties of Pure DLC and Si-DLC coatings, including silicon content, surface roughness, hardness, Young's modulus, and sp3 carbon content.

DLC Name	Si [at. %]	Roughness: R_a [nm]	Hardness [GPa]	Young Modulus [GPa]	sp^3 content [%]
Pure DLC	0	4.9 ± 0.1	15.6 ± 0.6	167 ± 3	26
Si-DLC	14.4	5.2 ± 0.2	19.4 ± 0.6	204 ± 4	56

2.2. Lubricants

Lauryl methacrylate (LMA) and 2-dimethylaminoethyl methacrylate (DMAEMA) copolymers were synthesized via Supplemental Activator and Reducing Agent Atom Transfer Radical Polymerisation (SARA ATRP) following a procedure described (Fig. 1) [16]. In brief, a Schlenk reactor was charged with copper wire and copper (II) bromide under nitrogen. Separately, a mixture of ethyl-α-bromophenyl acetate, LMA, *N,N,N,N,N*-pentamethyldiethylenetriamine, and anisole was prepared and purged with nitrogen. The reactor was then placed in a preheated oil bath to allow the reaction to proceed for 3 h. The DMAEMA was then added for the synthesis of PLMA-*b*-PDMAEMA, and the reaction continued for another hour. To assess the tribological impact of the functional group, PLMA and PLMA-*b*-PDMAEMA were synthesized, and the DMAEMA content was determined by ^{1}H NMR (Table 2).

The polyalphaolefin 4 (PAO 4) used as the base lubricant was purchased from KEMAT. A mixture containing 8 wt% of the synthesized polymer was prepared by mixing 8 g of the polymer with 92 g of PAO 4. A defined volume (20 μL) of the polymer-PAO 4 mixture was drop-cast onto the center of each coated steel disk using a micropipette. The disks were allowed to rest for 5 min to ensure uniform spreading. The same procedure was followed for all samples to ensure reproducibility.

2.3. Tribological tests

The tribological tests were conducted using the Rtec MFT-5000 tribometer (Rtec Instruments) in a ball-on-disk reciprocating sliding configuration. A 3/8-inch SiC ball was employed, and the applied load was set to 3 N to achieve a Hertzian contact pressure of 1.0 GPa. Based on previous studies [19], the most effective friction reduction was observed at a low sliding velocity of 0.2 Hz (0.006 m/s) (Fig. 2). Therefore, the sliding tests to obtain the samples for further analysis by ToF-SIMS and XPS were performed at this velocity for a duration of 40 min. The stroke length was set to 15 mm, and the tests were conducted at a temperature of 80 °C. All surface characterizations were carried out after the tribological tests. The analyzed areas were selected from representative wear regions located at the center of each wear scar. The same procedure and location were used consistently for all samples to ensure reproducibility and comparability.

2.4. Surface analysis

2.4.1. ToF-SIMS analysis

ToF-SIMS (Time-of-Flight Secondary Ion Mass Spectrometry) was performed on a TOF.SIMS5 instrument (ION-TOF GmbH, Münster, Germany). The spectrometer is equipped with a Bi cluster primary ion source and a reflectron type time-of-flight analyzer. UHV base pressure was $<3 \times 10^{-8}$ mbar. For high mass resolution the Bi source was operated in "high current bunched" mode providing short Bi_3^+ primary ion pulses at 25 keV energy, a lateral resolution of approx. 4 μm, and a target current of 0.34 pA at a cycle time of 100 μs. The short pulse length of 1.3 ns allowed for high mass resolution. The primary ion beam was scanned across a 500 × 500 μm^2 field of view on the sample, and 128 × 128 data points were recorded. Primary ion doses were kept at 2×10^{11} ions/cm^2 (static SIMS limit). Spectra were calibrated on the omnipresent C^-, CH^-, CH_2^-, C_2^-, C_3^-, or on the CH^+, CH_2^+, and CH_3^+, $C_2H_3^+$, and $C_3H_5^+$ peaks. Based on these datasets the chemical assignments for characteristic fragments were determined. For data evaluation the area of the wear scar was used (70 × 500 μm^2), if not stated otherwise.

For depth profiling a dual beam analysis was performed in interlaced mode: The primary ion source was again operated in "high current

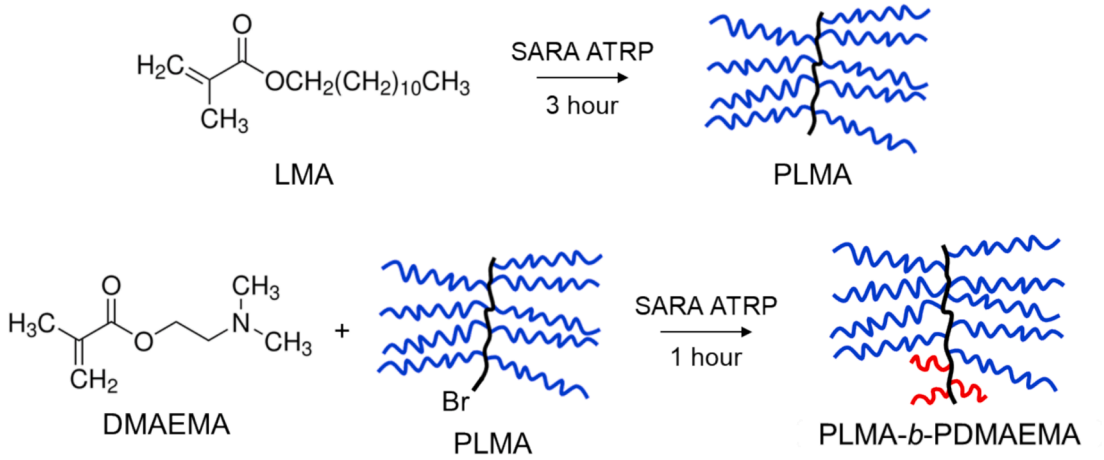

Fig. 1. Molecular structures of PLMA and PLMA-*b*-PDMAEMA used as lubricant additives. The presence of PDMAEMA blocks introduces amine functionality, which plays a key role in tribofilm formation on Si-DLC surfaces.

Table 2
Molecular characteristics of the synthesized PLMA and PLMA-*b*-PDMAEMA copolymers, including the molar ratio of PDMAEMA, number-average molecular weight (M_w), and polydispersity index (M_w/M_n).

Polymer name	PDMAEMA amount [mol%]	M_w [kDa]	M_w/M_n
PLMA	0	25	1.07
PLMA-*b*-PDMAEMA	10	25	1.06

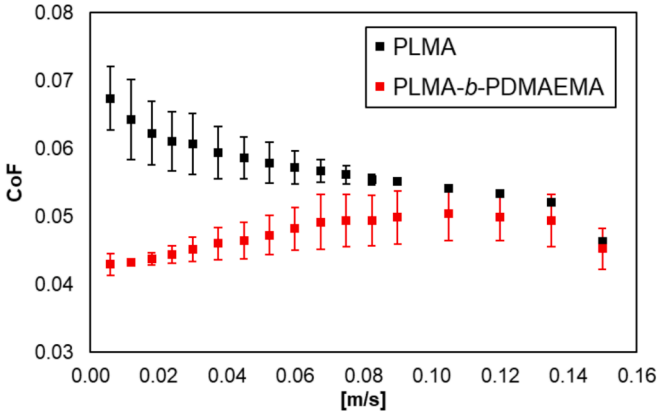

Fig. 2. Friction properties of PLMA and PLMA-*b*-PDMAEMA on Si-DLC with the standard deviation.

bunched" mode with a scanned area of 500 × 500 μm^2 and a sputter gun (operated with Ar^+_{1300} ions, 5 keV, scanned over a concentric field of 750 × 750 μm^2, target current 0.5nA) was applied to erode the sample. The accumulated ion fluence is used as an arbitrary measure for depth.

2.4.2. XPS analysis

X-ray Photoelectron Spectroscopy (XPS) was performed at the CIRCE-NAPP branch of BL24 at the synchrotron ALBA (Barcelona). The endstation [23,24] is equipped with a Phoibos NAP150 electron analyzer from SPECS, positioned at the Magic Angle. The available energy range at CIRCE is 90–2000 eV and the beam spot measures 100 × 20 (H × V) μm^2). The photons incidence angle was approximately 40°. The overall energy resolution in the experimental conditions (pass energy = 10 eV for core levels, 20 eV for surveys, exit slit 20 μm) was better than 0.3 eV. The binding energy was calibrated using 284.8 eV of C1s.

2.4.3. FIB-TEM analysis

Cross-sectional TEM lamellae were prepared using a Zeiss 550L cross-beam system. The wear track region of interest was first located using the in-situ SEM, and a protective platinum (Pt) layer was deposited on the surface by ion-beam induced deposition (IBID) to prevent damage from the Ga^+ ion beam during milling. Prior to FIB processing, a thin layer of gold (Au) had already been deposited on the sample surface as a conductive coating. Following Pt deposition, trenches were milled on both sides of the target region to define the lamella. Coarse milling was performed at high accelerating voltage (30 kV) and high beam currents, to obtain a 1 μm thick lamella. The lamella was then lifted out using an in-situ micromanipulator and attached to a Cu TEM grid using Pt deposition. Final thinning of the lamella to achieve electron transparency (~100 nm thickness) was also carried out at progressively lower energies (typically down to 5 kV or 2 kV) to reduce ion-beam damage, surface amorphization, and curtaining effect.

High-resolution transmission electron microscopy (HRTEM) and high-angle annular dark-field scanning transmission electron microscopy (HAADF-STEM) were performed using a Tecnai G2 F20 microscope operated at an accelerating voltage of 200 kV. This microscope was used to observe the cross-sectional structure of the wear track regions and to identify the layered morphology formed during tribological contact. To obtain higher spatial resolution and compositional information, complementary HAADF-STEM imaging, energy-dispersive X-ray spectroscopy (EDX) and electron energy loss spectroscopy (EELS) analyses were carried out using a Thermo Fisher Spectra 300 microscope operated at 300 kV, equipped with a SuperX detection system and a Gatan Continuum K3 EELS spectrometer with direct electron detection. Elemental maps for C and Si were collected to analyze the chemical distribution within the tribofilm and across the interface with the underlying Si-DLC layer.

3. Results and discussion

3.1. Chemical structure analysis of polymers

To characterize the chemical structure of the polymers at Si-C surfaces, ToF-SIMS was employed to analyze individual polymers. Several drops of a PLMA and a PLMA-*b*-PDMAEMA solution in hexane were deposited onto a silicon wafer and air dried, and the surfaces were analyzed. The resulting positive and negative secondary ion spectra are shown in Fig. 3. In Fig. 3, blue circles indicate peaks originating from PLMA, while red circles correspond to peaks derived from PLMA-*b*-PDMAEMA. In the negative ion spectra, both polymers exhibited peaks corresponding to $C_3H_3O^-$ ($m/z = 55$) and $C_4H_5O_2^-$ ($m/z = 85$), indicative

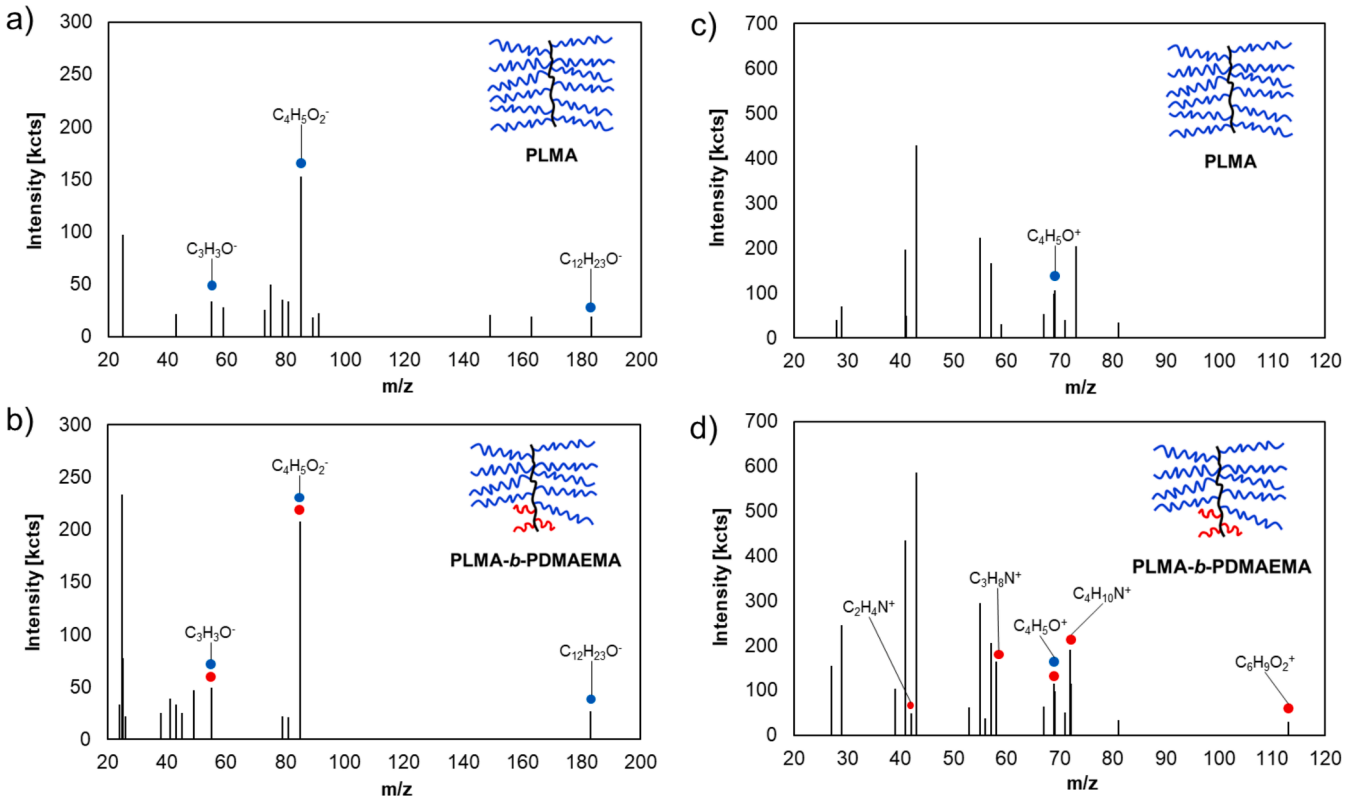

Fig. 3. Representative ToF-SIMS spectra of PLMA and PLMA-*b*-PDMAEMA drop-cast on Si wafers. (a) and (b) show negative ion spectra, while (c) and (d) show positive ion spectra. Characteristic ion fragments from PLMA are highlighted in blue, while those from the PDMAEMA-containing block copolymer are marked in red. These peaks serve as key chemical markers for identifying polymer-derived fragments in subsequent tribofilm analyses. (For interpretation of the references to colour in this figure legend, the reader is referred to the web version of this article.)

of the polymer backbone [25]. Additionally, a peak corresponding to $C_{12}H_{23}O^-$ (m/z = 183), representing the long carbon chain of PLMA, was observed in both polymers [25].

The differences between PLMA and PLMA-*b*-PDMAEMA were observed in the positive ion spectra. Specifically, characteristic peaks of PDMAEMA, such as $C_2H_4N^+$ (m/z = 42), $C_3H_8N^+$ (m/z = 58, hard to separate from the adjacent $C_4H_{10}^+$), $C_4H_{10}N^+$ (m/z = 72), $C_6H_9O_2^+$ (m/z = 113) were detected in the mass spectra of PLMA-*b*-PDMAEMA [26–30]. These results suggest that these positive peaks are valid markers for evaluating tribofilms on wear scars in the presence of PLMA-*b*-PDMAEMA.

3.2. *Friction behavior of polymers*

Tribological tests were performed on both Pure DLC and Si-DLC coatings in the presence of PLMA and PLMA-*b*-PDMAEMA.

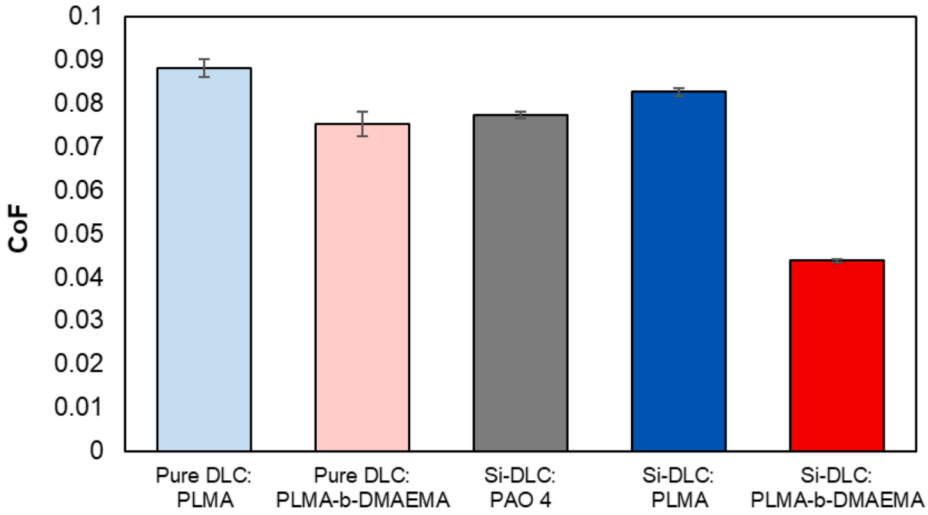

Fig. 4. Average coefficient of friction (CoF) during the final 5 min of tribological tests on Pure DLC and Si-DLC coatings, lubricated with PAO 4, PLMA, or PLMA-*b*-PDMAEMA. The results show that only PLMA-*b*-PDMAEMA significantly reduces friction on Si-DLC, highlighting the importance of amine functionality and surface reactivity. Tests were conducted at 80 °C under 1.0 GPa Hertzian contact pressure.

Additionally, a baseline experiment was conducted on Si-DLC using only the base oil (PAO 4) without any polymeric additives. The average coefficient of friction (CoF) recorded during the final five minutes of the 40-minute test is presented in Fig. 4. In the case of the pure DLC coatings, the presence of functional groups in the functionalized copolymer did not lead to a significant change in the frictional behavior. In contrast, for the Si-DLC coatings, replacing only the base oil (PAO 4) with PLMA did not lead to any appreciable effect, while PLMA-*b*-PDMAEMA caused a significant reduction in friction. Furthermore, the CoF in the presence of PLMA-*b*-PDMAEMA, remained relatively stable throughout the tests for both coatings (see **Fig. S1** in the Supplementary Information). These results indicate the effectiveness of PLMA-*b*-PDMAEMA in reducing friction on Si-DLC coatings, likely due to enhanced interactions between its functional groups and reactive silicon sites.

3.3. Surface analysis of wear scars using ToF-SIMS

The surface analysis of the wear scars was carried out after the tribological tests. First, static ToF-SIMS analyses were performed on each wear scar, focusing on positive secondary ion peaks. The $C_2H_4N^+$ ($m/z = 42$) peak was used to compare the amount of DMAEMA amine groups on the surface, (Fig. 5**(a)**), as other nitrogen-containing peaks, such as $C_3H_8N^+$ and $C_4H_{10}N^+$, overlap with carbon chain peaks such as $C_4H_{10}^+$ and $C_5H_{12}^+$. The results showed that the amount of nitrogen-containing species in the wear scars was lower in PAO 4 alone or in the presence of pure PLMA, while the combination of PLMA-*b*-PDMAEMA and Si-DLC had the highest amount of nitrogen-containing species. Next, the $C_4H_5O^+$ peak ($m/z = 69$) was analyzed to compare the amount of polymer backbone, as shown in Fig. 5**(b)**. It was found that more polymer backbone was present in the wear scars when PLMA-*b*-PDMAEMA was used compared to PLMA, and this effect was more pronounced for Si-DLC coatings. It is also noteworthy noting that in the case of PAO 4 alone, the presence of $C_4H_5O^+$ was negligible. In the negative ion spectra, the intensity of the peaks corresponding to the polymer backbone also showed trends consistent with those of the positive ion spectra (**Fig. S2**).

For a more detailed analysis, the depth profiles of the positive peaks in the presence of PLMA-*b*-PDMAEMA on pure DLC and Si-DLC are shown in Fig. 6. It is evident that the $C_2H_4N^+$ ($m/z = 42$) and $C_4H_5O^+$ ($m/z = 69$) peaks are more abundant on Si-DLC, particularly near the surface. These findings suggest that the interaction between PLMA-*b*-PDMAEMA and Si-DLC promotes the formation of a tribofilm enriched in nitrogen-containing species, which may contribute to the observed friction reduction.

The depth-dependent evolution of the characteristic fragments within the tribofilm formed on Si-DLC in the presence of PLMA-*b*-PDMAEMA was evaluated (Fig. 7). The depth profiles of the Si^+, $C_2H_4^+$, $C_4H_5O^+$, and $C_{12}H_{23}O^-$ peaks were normalized such that the maximum

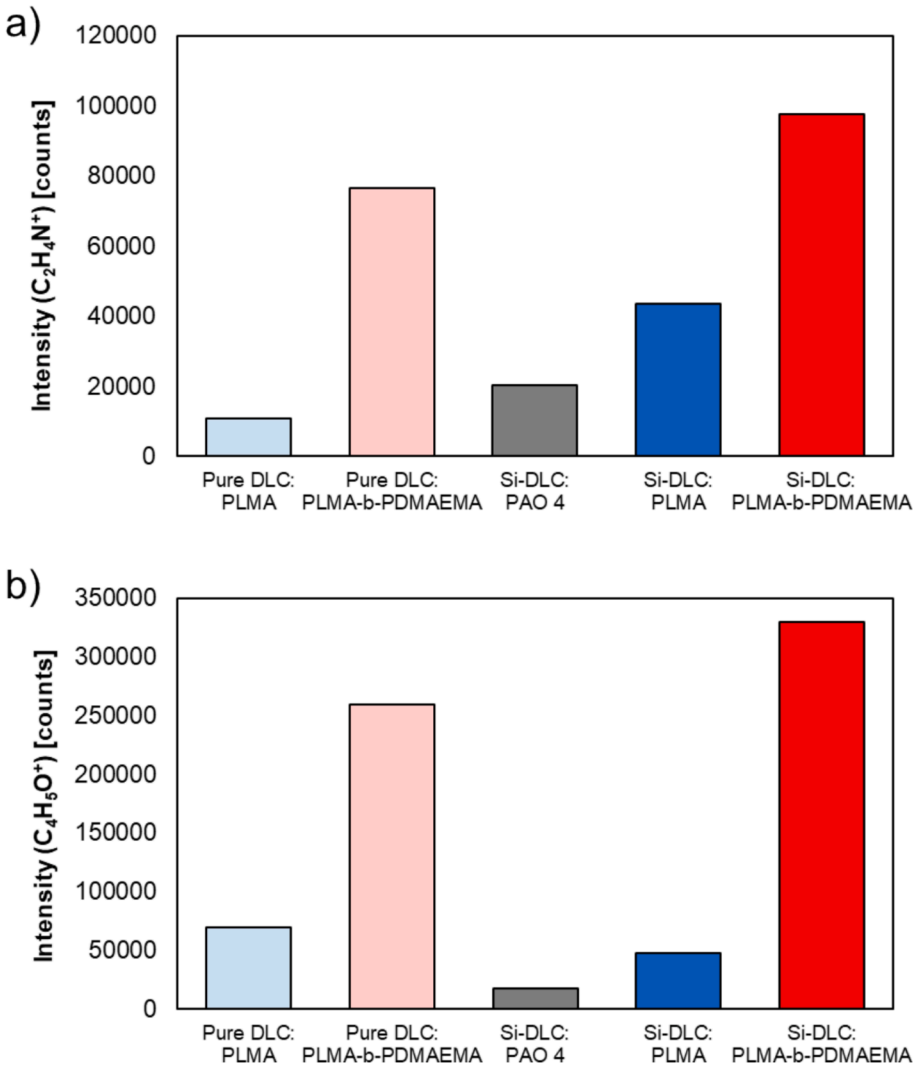

Fig. 5. Static ToF-SIMS: Comparison of (a) $C_2H_4N^+$ ($m/z = 42$) and (b) $C_4H_5O^+$ ($m/z = 69$) peak intensity in wear scars for PLMA and PLMA-*b*-PDMAEMA on Pure DLC and Si-DLC surface, with PAO 4 on Si-DLC serving as the benchmark.

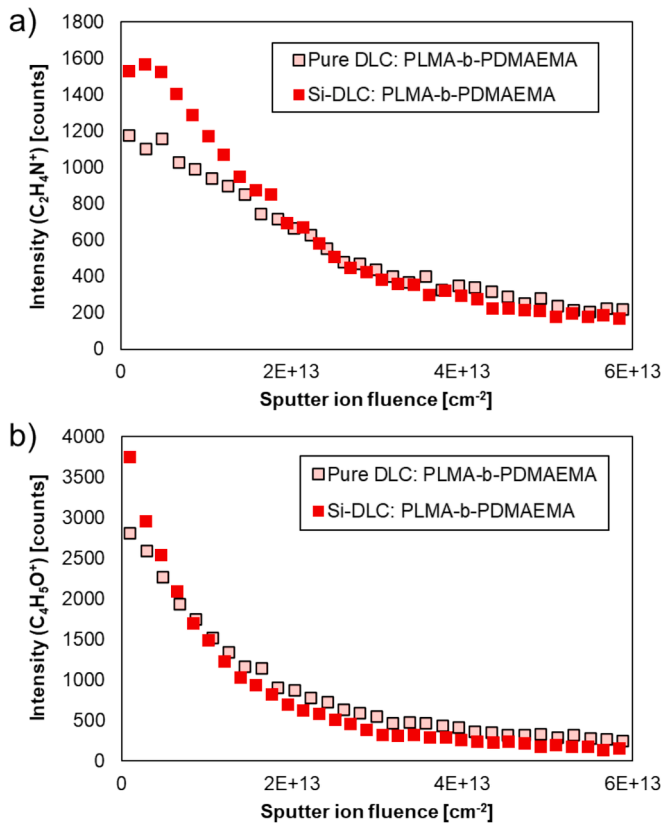

Fig. 6. Depth profiles of (a) $C_2H_4N^+$ (m/z = 42) and (b) $C_4H_5O^+$ (m/z = 69) peaks on Pure DLC and Si-DLC in the presence of PLMA-*b*-PDMAEMA.

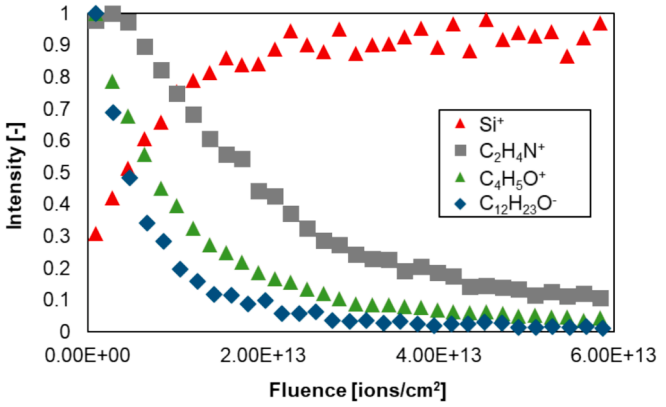

Fig. 7. Depth profiles of relative intensities for Si^+, $C_2H_4N^+$, $C_4H_5O^+$, and $C_{12}H_{23}O^-$ within the wear scar formed on Si DLC in the presence of PLMA-*b*-PDMAEMA.Each peak intensity was normalized to its respective maximum value (set to 1).

intensity of each peak was set to 1. The results show that the intensity of $C_{12}H_{23}O^-$, $C_4H_5O^+$, and $C_2H_4^+$ signals gradually decrease, while the Si^+ signal from the underlying Si-DLC coating becomes more prominent. Once Si^+ stabilizes, the other peaks become negligible. This observation suggests that the long alkyl chain of PLMA ($C_{12}H_{23}O^-$) is mainly located at the outermost surface. Thereafter, the backbone fragment ($C_4H_5O^+$) which is common to both PLMA and PDMAEMA begins to decrease. The amine-related fragment of PDMAEMA ($C_2H_4N^+$) remains closer to the interface between the tribofilm and the coating, indicating that the amine groups persist over most of the tribofilm depth.

In order to compare the differences in the composition of the tribofilm, a comparison was made with the polymer alone. Fig. 8 shows a

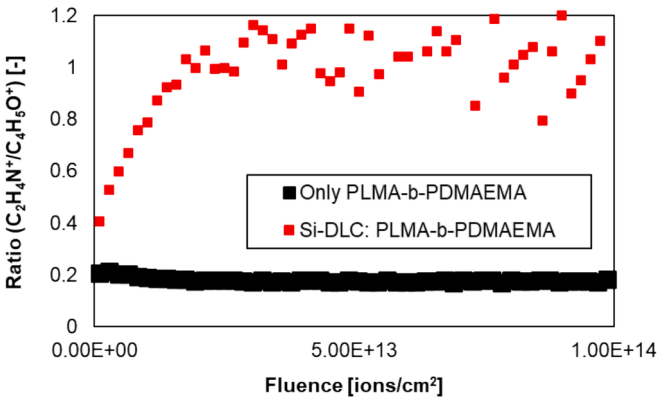

Fig. 8. Depth profiles of the ratio of amine groups ($C_2H_4N^+$) point-to-point normalized to polymer backbone signal ($C_4H_5O^+$), comparing the polymer alone (drop cast onto Si wafer, representing a bulk copolymer sample) with the tribofilm formed in the presence of PLMA-*b*-PDMAEMA on Si-DLC.

depth comparison between the polymer alone and the tribofilm formed on Si DLC in the presence of PLMA-*b*-PDMAEMA. The ratio of the amine groups ($C_2H_4N^+$) to the polymer backbone ($C_4H_5O^+$) was calculated as a function of depth. When the polymer alone was applied, this ratio remained nearly constant at about 0.2 throughout the depth. In contrast, the ratio in the tribofilm, gradually increased with depth eventually approaching 1. These results indicate that the amine groups within the tribofilm exhibit preferential adsorption to Si-DLC, which differs from the behavior observed when the polymer itself is applied.

To further illustrate the proposed mechanism, schematic diagrams are presented in Fig. 9. As shown in Fig. 9**(a)**, when the PLMA-*b*-PDMAEMA copolymer is deposited on the Si wafer without sliding, the molecular arrangement remains random, and the amine groups are uniformly distributed. In contrast, Fig. 9**(b)** depicts the situation after sliding on the Si-DLC surface, where tribological stress and interfacial interaction with silicon atoms promote the selective localization of the amine-containing PDMAEMA segments near the interface. This rearrangement under shear is consistent with the increasing $C_2H_4N^+/C_4H_5O^+$ ratio observed in the depth profile and suggests the formation of a compositionally graded tribofilm anchored by N–Si bonding.

3.4. *Chemical bonding analysis of tribofilms using synchrotron-based XPS*

The chemical bonding states in the tribofilms that had formed on the wear scars were then elucidated using synchrotron-based XPS. By adjusting the photon energy, it is possible to examine different sampling

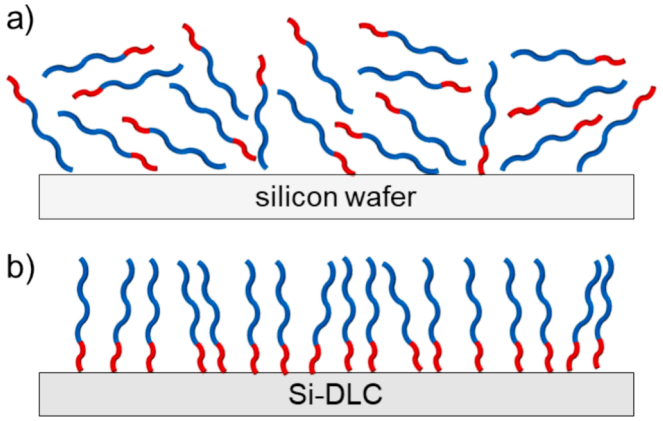

Fig. 9. Schematic representation of (a) the polymer film morphology after drop-casting PLMA-*b*-PDMAEMA on the Si wafer without sliding and (b) the tribofilm formed on Si-DLC after sliding.

depths, enabling depth-resolved analysis of the tribofilm. Increasing the photon energy raises the kinetic energy of the emitted photoelectrons, allowing signals from deeper regions to be detected. Focusing on the silicon peaks, two different bonding states were identified, Si-C bonds (peak at 100.8 ± 0.2 eV) and Si-O-C bonds (peak at 102.6 ± 0.2 eV) [18] (**Fig. S3**). The evolution of these peaks at different photon energies is show in Fig. 10**(a)**. The results indicate that with increasing depth, the intensity of the Si-C bonds increases while that of the Si-O-C bonds decreases. This trend indicates that the surface is covered by an oxide layer, which changes into a more carbide-rich layer with increasing depth.

Next, attention was focused on the nitrogen XPS peaks. Two nitrogen-related binding states were detected, N-Si bonds (peak at 398.8 ± 0.2 eV) and N-C bonds (peak at 399.8 ± 0.2 eV) [31,32] (**Fig. S4**). The depth-dependent changes of these peaks are shown in Fig. 10**(b)**. With increasing the probing depth, the relative intensity of the N-C bonds decreased, while the relative intensity of the N-Si bonds increased. It is noteworthy that at a photon energy of about 700 eV, both intensities reach a steady state. Considering that N-C bonds indicate the amine groups of PDMAEMA, and N-Si bonds reflect the adsorption of PDMAEMA on the Si-DLC surface, these results suggest that the outermost surface is enriched with amine groups of PDMAEMA, while in the depth of the tribofilm, the fraction of N-Si bonds gradually increases.

In addition, changes in the carbon bonding states were investigated. The C 1 s spectrum was fitted into six components, which correspond to C-Si (283.5 ± 0.2 eV), C–C sp^2 (284.6 ± 0.2 eV), C–C sp^3 (285.3 ± 0.2 eV), C-O (286.6 ± 0.2 eV), C=O (288.0 ± 0.2 eV), and O-C=O (288.8 ± 0.2 eV) as shown in **Fig. S5** and reported in previous literature [33–39]. A depth-dependent variation of C–C and oxygen-containing carbon bonds (C–O and C=O) was observed, as shown in **Fig. S6**. However, the overall change was around 4 percent, which is within the potential margin of error for multi-peak fitting. Therefore, the trends in carbon bonding are less conclusive compared to the more prominent depth-related changes observed in the silicon and nitrogen signals. These results are presented in the Supplementary Information for reference.

In the subsequent analysis, the atomic ratios in the tribofilm were determined using unified kinematic energies of 450 eV and 900 eV. Furthermore, the detection depth corresponding to these kinematic energies was estimated using the IMFP-TPP2M software [40–42]. Fig. 10 **(c)** shows the depth-dependent changes of the nitrogen and silicon peaks, which exhibit the strongest variation with photon energy. The results show that the N-Si signal stabilizes near 6 nm from the surface, while the Si-O-C peak, which corresponds to the oxide layer, begins to decrease. This observation suggests that the boundary between the tribofilm and the underlying Si-DLC substrate lies at this depth.

Table 3 presents the atomic ratios at each depth. The results clearly indicate that, at greater depths, the amounts of nitrogen and silicon increase. One possible explanation for this trend is that the tribofilm's subsurface layers contain nitrogen-rich compounds, which could have formed through adsorption processes.

This depth-dependent N–Si bonding behavior is consistent with previous studies on amine-functionalized polymers interacting with oxide-terminated DLC surfaces [19,20], suggesting a general mechanism for anchoring under tribological conditions. The formation of chemically anchored N–Si bonds not only stabilizes the interfacial structure but likely contributes to the reduced wear and friction observed in Fig. 4, by maintaining film integrity under sliding.

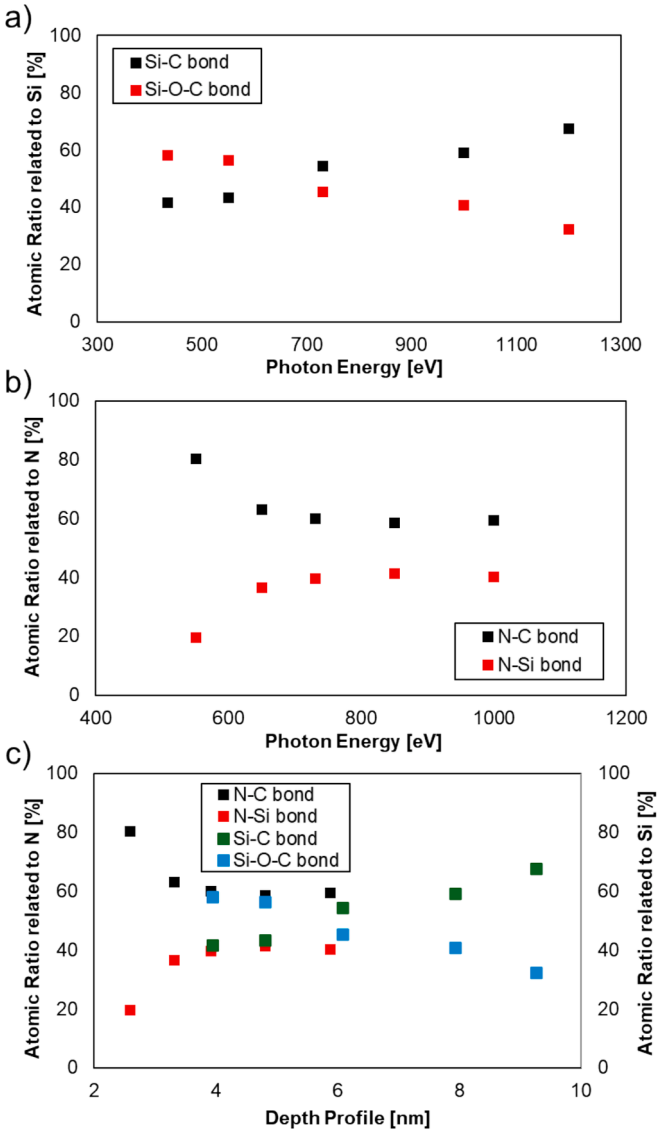

Fig. 10. Depth-resolved synchrotron-based XPS analysis of the tribofilm formed on Si-DLC after lubrication with PLMA-b-PDMAEMA, measured at kinetic energies of 450 and 900 eV. (a) Evolution of Si–C and Si–O–C bonding components. The Si–C contribution increases with depth, indicating a transition from surface oxidation to a more carbide-rich subsurface. (b) N–C and N–Si bond fractions as a function of sampling depth. The dominance of N–C near the surface and the increase of N–Si with depth suggest that PDMAEMA segments first adsorb via amine groups and then chemically anchor to the Si-DLC substrate. (c) Quantitative atomic concentrations of nitrogen and silicon, showing an enrichment of both elements at greater depths, consistent with the formation of an interfacial region stabilized by N–Si bonding.

3.5. *FIB-TEM analysis of the tribofilm on Si-DLC*

Cross-sectional FIB-TEM analysis clarified the morphology and thickness of the tribofilm formed on the Si-DLC surface in the presence of PLMA-*b*-PDMAEMA. Fig. 11**(a)** shows a representative HAADF image in which a protective Pt layer is deposited on top of a thin Au film. The Au film was deposited prior to Pt deposition to safeguard the tribofilm from collapse during the subsequent Pt coating step. Below these layers, a

Table 3
Atomic composition of the tribofilm at different sampling depths, derived from XPS measurements using kinematic energies of 450 eV and 900 eV. The data show increasing nitrogen and silicon content with depth, supporting the formation of an N–Si rich interfacial layer that anchors the tribofilm to the Si-DLC substrate.

Kinematic Energy [eV]	450	900
Depth Profile [nm]	4.8	7.9
N [at. %]	0.1	5.6
C [at. %]	97.1	87.4
Si [at. %]	2.7	7.0

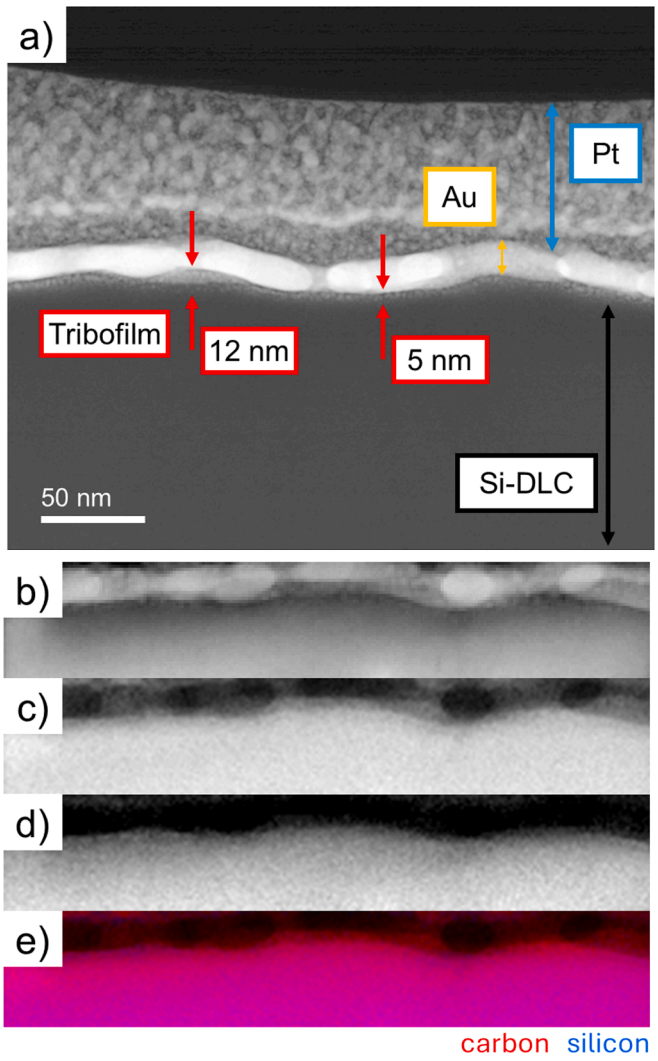

Fig. 11. Cross-sectional FIB-TEM and EDX elemental mapping of the tribofilm formed on Si-DLC after sliding in the presence of PLMA-*b*-PDMAEMA. (a) Cross-sectional HAADF image of the tribofilm formed on Si-DLC after sliding in the presence of PLMA-b-PDMAEMA. (b) HAADF image of the cross section, (c) elemental map showing the distribution of carbon, (d) elemental map showing the distribution of silicon, and (e) overlay of carbon (red) and silicon (blue), illustrating a carbon-enriched tribofilm layer on top of the silicon-containing DLC. (For interpretation of the references to colour in this figure legend, the reader is referred to the web version of this article.)

distinct tribofilm can be seen over the Si-DLC substrate. The tribofilm thickness ranges from 5 to 12 nm, closely matching the ~6 nm depth estimated by synchrotron-based XPS.

Fig. 11 shows HAADF imaging and elemental maps. The carbon signal in Fig. 11**(c)** appears similarly intense in both the tribofilm and the Si-DLC, reflecting their carbon-rich nature. Fig. 11**(d)** shows that silicon can only be detected in the Si-DLC layer. Fig. 11**(e)** overlays the carbon and silicon maps, confirming that the silicon-doped layer lies beneath a carbon-based film. These observations demonstrate that a polymer-derived tribofilm forms on the Si-DLC and that its thickness agrees well with the XPS results, supporting the interpretation that the amine-containing segments of PLMA-*b*-PDMAEMA are anchored to the silicon-doped surface, while the alkyl segments forms a low-friction surface layer.

3.6. Mechanism of tribofilm formation on Si-DLC

The proposed mechanism for the tribofilm formation on Si-DLC in the presence of PLMA-*b*-PDMAEMA is shown in Fig. 12. The tribofilm is characterized by a layered structure consisting of polymeric components adsorbed on the Si-DLC surface. This structure plays a critical role in reducing friction and improving wear resistance.

In the outermost layer, the long alkyl chains of the PLMA segment (indicated as $C_{12}H_{23}O^-$) are oriented outwards and forms a low-shear interface that interacts effectively with the lubricant medium. These chains form a highly oleophilic surface that minimizes direct contact between the surfaces and reduces friction during sliding.

Beneath the alkyl chain layer are the polymer backbone fragments (indicated as $C_4H_5O^+$) which form the structural basis of the tribofilm. These components contribute to the overall integrity and mechanical stability of the tribofilm under high loading conditions. In comparison, the $C_2H_4N^+$ signal shows a shallower slope in the depth profile (Fig. 7), indicating that the amine groups from the PDMAEMA segment are more concentrated in the bottom part of the tribofilm. These functional groups exhibit strong interactions with the Si-DLC surface, likely forming stable chemical or coordination bonds. This depth-dependent accumulation supports the interpretation that the amine-containing PDMAEMA segments anchor the tribofilm to the Si-DLC coating via N–Si bonding. Such interactions are essential for ensuring strong adhesion to the substrate and maintaining the durability of the tribofilm during sliding.

The observed structure of the tribofilm explains the superior tribological performance observed in the presence of PLMA-*b*-PDMAEMA. The outermost oleophilic layer reduces shear stress, while the amine-rich inner layer improves adhesion to the Si-DLC surface, preventing delamination of the film. This layer architecture ensures stable friction reduction and effective wear protection, even under demanding lubrication conditions.

4. Conclusion

This study elucidates the detailed structure and performance of a tribofilm responsible for the enhanced tribological behavior of a novel lubrication system that combines PLMA-*b*-PDMAEMA block copolymers

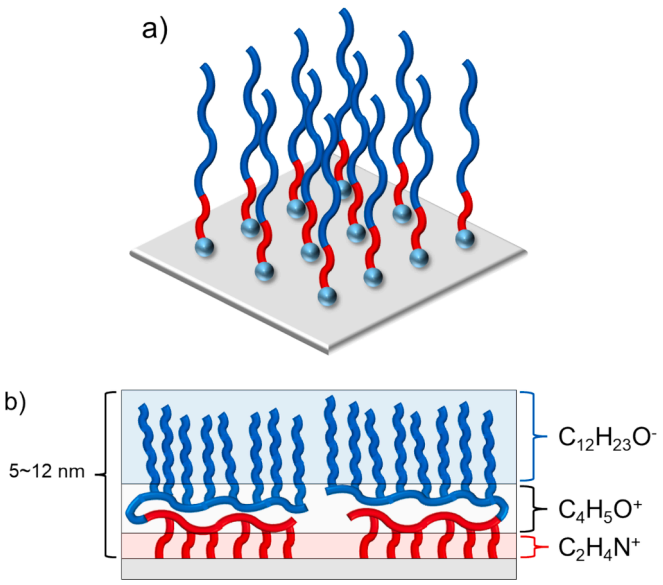

Fig. 12. Adsorption and Tribofilm Formation Mechanism on Si-DLC with PLMA-b-PDMAEMA. (a) Illustration of the adsorption process of PLMA-*b*-PDMAEMA on Si-DLC, showing red schematics representing PDMAEMA (amine groups) and blue schematics representing PLMA (alkyl chains). (b) Fully formed tribofilm structure after sliding, highlighting the layered configuration with PDMAEMA segments interacting strongly with the Si-DLC surface and PLMA segments forming the outer oleophilic layer. (For interpretation of the references to colour in this figure legend, the reader is referred to the web version of this article.)

with Si-DLC coatings. Comprehensive surface analyses, including ToF-SIMS, synchrotron-based XPS, and cross-sectional FIB-TEM, confirmed the in-situ formation of a polymer-derived tribofilm with a thickness of approximately 5–12 nm on the Si-DLC surface. The tribofilm remained stable under a Hertzian contact pressure of approximately 1 gigapascal, demonstrating mechanical robustness under severe boundary lubrication conditions. The tribofilm exhibits a chemically stratified structure. The amine functionalities of the PDMAEMA segment are strongly anchored to the silicon-rich substrate through N–Si chemisorption, while the long alkyl chains of the PLMA segment extend outward into the lubricant phase, forming a low-shear and oleophilic outer layer. This dual-layer configuration suppresses direct asperity contact, leading to reduced friction and improved wear protection.

The correlation between polymer functionality, particularly the presence of amine groups, and tribofilm formation underscores the importance of precise copolymer design for the development of metal-free lubrication systems. The present findings provide a mechanistic foundation for designing next-generation lubricant additives that achieve stable and low-friction performance on doped DLC surfaces, offering a more sustainable alternative to conventional phosphorus and sulfur-containing additives.

CRediT authorship contribution statement

Takeru Omiya: Writing – original draft, Visualization, Validation, Methodology, Investigation, Formal analysis, Data curation, Conceptualization. **Alexander Welle:** Writing – review & editing, Software, Methodology, Formal analysis, Data curation. **Manuel Evaristo:** Investigation. **Pooja Sharma:** Writing – review & editing, Data curation. **Albano Cavaleiro:** Writing – review & editing, Resources, Funding acquisition, Conceptualization. **Arménio C. Serra:** Writing – review & editing, Resources, Funding acquisition. **Jorge F.J. Coelho:** Writing – review & editing, Supervision, Resources, Project administration, Funding acquisition, Conceptualization. **Maria Clelia Righi:** Writing – review & editing, Supervision, Resources, Project administration, Investigation, Funding acquisition, Conceptualization. **Fabio Ferreira:** Writing – review & editing, Supervision, Resources, Project administration, Funding acquisition, Conceptualization.

Declaration of competing interest

The authors declare that they have no known competing financial interests or personal relationships that could have appeared to influence the work reported in this paper.

Acknowledgments

This research is sponsored by national funds through FCT – Fundação para a Ciência e a Tecnologia, under the projects UID/00285 - Centre for Mechanical Engineering, Materials and Processes, LA/P/0112/2020, 2023.08138.CEECIND/CP2832/CT0005, SmartHyLub (2022.05603.PTDC), iLub (2022.15609.UTA), UniLub (2023.17357.ICDT) and by the Taiho Kogyo Tribology Research Foundation (Grant No. 22A25). This project has received funding from the European Union's Horizon 2020 research and innovation programme under grant agreement No 101007417, having benefited from the access provided by ALBA Synchrotron, Barcelona; Karlsruhe Institute of Technology, Karlsruhe; Consejo Superior de Investigaciones Científicas - Centro Nacional de Microelectrónica, Barcelona; Fundacio Institut Català de Nanociència i Nanotecnologia, Barcelona within the framework of the NFFA-Europe Pilot Transnational Access Activity, proposal ID580.

Funded by the European Union

These results are part of the "Advancing Solid Interface and Lubricants by First Principles Material Design (SLIDE)" project that has received funding from the European Research Council (ERC) under the European Union's Horizon 2020 research and innovation program (Grant agreement No. 865633).

Appendix A. Supplementary material

Supplementary data to this article can be found online at https://doi.org/10.1016/j.apsusc.2025.164200.

Data availability

Data will be made available on request.

References

[1] P.J. Blau, Friction, lubrication, and wear technology, 1992.
[2] L. Zhou, J. Li, F. Li, Q. Meng, J. Li, X. Xu, Energy consumption model and energy efficiency of machine tools: a comprehensive literature review, J. Clean. Prod. 112 (2016) 3721–3734.
[3] K. Holmberg, A. Erdemir, Influence of tribology on global energy consumption, costs and emissions, Friction 5 (2017) 263–284.
[4] F. Bowden, J. Gregory, D. Tabor, Lubrication of metal surfaces by fatty acids, Nature 156 (3952) (1945) 97–101.
[5] Y. Yamamoto, S. Gondo, T. Kamakura, N. Tanaka, Frictional characteristics of molybdenum dithiophosphates, Wear 112 (1) (1986) 79–87.
[6] J. Graham, H. Spikes, S. Korcek, The friction reducing properties of molybdenum dialkyldithiocarbamate additives: part I—factors influencing friction reduction, Tribol. Trans. 44 (4) (2001) 626–636.
[7] A.M. Barnes, K.D. Bartle, V.R. Thibon, A review of zinc dialkyldithiophosphates (ZDDPS): characterisation and role in the lubricating oil, Tribol. Int. 34 (6) (2001) 389–395.
[8] K. Kimura, M. Lynskey, E.R. Corrigan, D.L. Hickman, J. Wang, H.L. Fang, S. Chatterjee, Real world study of diesel particulate filter ash accumulation in heavy-duty diesel trucks, SAE Technical Paper, 2006.
[9] A. Sappok, R. Rodriguez, V. Wong, Characteristics and effects of lubricant additive chemistry on ash properties impacting diesel particulate filter service life, SAE Int. J. Fuels Lubr. 3 (1) (2010) 705–722.
[10] M.J.S. De Carvalho, P.R. Seidl, C.R.P. Belchior, J.R. Sodré, Lubricant viscosity and viscosity improver additive effects on diesel fuel economy, Tribol. Int. 43 (12) (2010) 2298–2302.
[11] M.J. Covitch, K.J. Trickett, How polymers behave as viscosity index improvers in lubricating oils, Adv. Chem. Eng. Sci. 05 (02) (2015) 134–151.
[12] S. Gunsel, M. Smeeth, H. Spikes, Friction and wear reduction by boundary film-forming viscosity index improvers, SAE Trans. (1996) 1831–1855.
[13] M. Smeeth, H. Spikes, S. Gunsel, Boundary film formation by viscosity index improvers, Tribol. Trans. 39 (3) (1996) 726–734.
[14] M. Muller, K. Topolovec-Miklozic, A. Dardin, H.A. Spikes, The design of boundary film-forming PMA viscosity modifiers, Tribol. Trans. 49 (2) (2006) 225–232.
[15] J. Fan, M. Müller, T. Stöhr, H.A. Spikes, Reduction of friction by functionalised viscosity index improvers, Tribol. Lett. 28 (3) (2007) 287–298.
[16] T. Omiya, F. De Bon, T. Vuchkov, A. Serra, A. Cavaleiro, J. Coelho, F. Ferreira, Wear resistance by copolymers with controlled structure under boundary lubrication conditions, Lubr. Sci. 36 (1) (2024) 1–8.
[17] J. Vetter, 60 years of DLC coatings: Historical highlights and technical review of cathodic arc processes to synthesize various DLC types, and their evolution for industrial applications, Surf. Coat. Technol. 257 (2014) 213–240.
[18] M. Evaristo, R. Azevedo, C. Palacio, A. Cavaleiro, Influence of the silicon and oxygen content on the properties of non-hydrogenated amorphous carbon coatings, Diam. Relat. Mater. 70 (2016) 201–210.
[19] T. Omiya, E. Pedretti, M. Evaristo, A. Cavaleiro, A.C. Serra, J.F. Coelho, F. Ferreira, M.C. Righi, Synergistic effects of nitrogen-containing functionalized copolymer and silicon-doped DLC for friction and wear reduction, Tribol. Int. 200 (2024) 110183.
[20] T. Omiya, E. Pedretti, A. Cavaleiro, R. Gouttebaron, A. Felten, A.C. Serra, J. F. Coelho, M.C. Righi, F. Ferreira, Elucidating the composition and formation mechanism of slippery films from block copolymers on doped diamond-like carbon surfaces, Appl. Surf. Sci. 163599 (2025).
[21] A.C. Ferrari, J. Robertson, Raman spectroscopy of amorphous, nanostructured, diamond-like carbon, and nanodiamond, Philos. Trans. A Math Phys. Eng. Sci. 362 (1824) (2004) 2477–2512.

[22] W. Cui, Q. Lai, L. Zhang, F. Wang, Quantitative measurements of sp3 content in DLC films with Raman spectroscopy, Surf. Coat. Technol. 205 (7) (2010) 1995–1999.
[23] V. Pérez-Dieste, L. Aballe, S. Ferrer, J. Nicolàs, C. Escudero, A. Milán, E. Pellegrin, Near ambient pressure XPS at ALBA, J. Phys.: Conf. Series, IOP Publishing (2013) 072023.
[24] D. Ruano Sánchez, Caracterización de catalizadores basados en cobre en condiciones de reacción mediante técnicas espectroscópicas in situ, TDX (Tesis Doctorals en Xarxa), 2021.
[25] S. Clarke, M.C. Davies, C.J. Roberts, S.J. Tendler, P.M. Williams, V. O'Byrne, A. L. Lewis, J. Russell, Surface mobility of 2-methacryloyloxyethyl phosphorylcholine-co-lauryl methacrylate polymers, Langmuir 16 (11) (2000) 5116–5122.
[26] P. Lazzeri, L. Vanzetti, M. Anderle, M. Bersani, J. Park, Z. Lin, R. Briber, G. Rubloff, H. Kim, R. Miller, Thin-film transformations and volatile products in the formation of nanoporous low-k polymethylsilsesquioxane-based dielectric, J. Vacuum Sci. Technol. B: Microelectron. Nanometer Struct. Process. Measurement Phenomena 23 (3) (2005) 908–917.
[27] Q. Peng, D.M.Y. Lai, E.T. Kang, K.G. Neoh, Preparation of polymer−silicon(100) hybrids via interface-initiated reversible addition-fragmentation chain-transfer (RAFT) polymerization, Macromolecules 39 (16) (2006) 5577–5582.
[28] M. Tohyama, T. Ohmori, A. Murase, M. Masuko, Friction reducing effect of multiply adsorptive organic polymer, Tribol. Int. 42 (6) (2009) 926–933.
[29] P. Teper, J. Chojniak-Gronek, A. Hercog, N. Oleszko-Torbus, G. Płaza, J. Kubacki, K. Balin, A. Kowalczuk, B. Mendrek, Nanolayers of poly (N, N′-Dimethylaminoethyl methacrylate) with a star topology and their antibacterial activity, Polymers 12 (1) (2020) 230.
[30] M. Flejszar, K. Ślusarczyk, A. Hochół, P. Chmielarz, M. Wytrwal, K. Wolski, K. Spilarewicz, K. Awsiuk, J. Raczkowska, Sequential SI-ATRP in μL-scale for surface nanoengineering: a new concept for designing polyelectrolyte nanolayers formed by complex architecture polymers, Eur. Polym. J. 194 (2023) 112142.
[31] G.-R. Yang, Y.-P. Zhao, Y. Hu, T.P. Chow, R.J. Gutmann, XPS and AFM study of chemical mechanical polishing of silicon nitride, Thin Solid Films 333 (1–2) (1998) 219–223.
[32] Z.-W. Deng, R. Souda, XPS studies on silicon carbonitride films prepared by sequential implantation of nitrogen and carbon into silicon, Diam. Relat. Mater. 11 (9) (2002) 1676–1682.
[33] G.D. Sorarù, G. D'Andrea, A. Glisenti, XPS characterization of gel-derived silicon oxycarbide glasses, Mater. Lett. 27 (1–2) (1996) 1–5.
[34] Y. Hijikata, H. Yaguchi, M. Yoshikawa, S. Yoshida, Composition analysis of SiO2/SiC interfaces by electron spectroscopic measurements using slope-shaped oxide films, Appl. Surf. Sci. 184 (1–4) (2001) 161–166.
[35] X. Yan, T. Xu, S. Yang, H. Liu, Q. Xue, Characterization of hydrogenated diamond-like carbon films electrochemically deposited on a silicon substrate, J. Phys. D Appl. Phys. 37 (17) (2004) 2416.
[36] G. Wan, P. Yang, R.K. Fu, Y. Mei, T. Qiu, S. Kwok, J.P. Ho, N. Huang, X. Wu, P. K. Chu, Characteristics and surface energy of silicon-doped diamond-like carbon films fabricated by plasma immersion ion implantation and deposition, Diam. Relat. Mater. 15 (9) (2006) 1276–1281.
[37] A. Bendavid, P. Martin, C. Comte, E. Preston, A. Haq, F.M. Ismail, R. Singh, The mechanical and biocompatibility properties of DLC-Si films prepared by pulsed DC plasma activated chemical vapor deposition, Diam. Relat. Mater. 16 (8) (2007) 1616–1622.
[38] M.H. Ahmed, J.A. Byrne, J. McLaughlin, W. Ahmed, Study of human serum albumin adsorption and conformational change on DLC and silicon doped DLC using XPS and FTIR spectroscopy, (2013).
[39] Y.L. Khung, S.H. Ngalim, A. Scaccabarozzi, D. Narducci, Formation of stable Si–O–C submonolayers on hydrogen-terminated silicon (111) under low-temperature conditions, Beilstein J. Nanotechnol. 6 (1) (2015) 19–26.
[40] S. Tanuma, C.J. Powell, D.R. Penn, Calculations of electron inelastic mean free paths. V. Data for 14 organic compounds over the 50–2000 eV range, Surface and Interface Analysis 21(3) (1994) 165-176.
[41] H. Shinotsuka, S. Tanuma, C.J. Powell, D.R. Penn, Calculations of electron inelastic mean free paths. X. Data for 41 elemental solids over the 50 eV to 200 keV range with the relativistic full Penn algorithm, Surf. Interface Anal. 47 (9) (2015) 871–888.
[42] F.A. Stevie, C.L. Donley, Introduction to X-ray photoelectron spectroscopy, J. Vac. Sci. Technol. A 38 (6) (2020).